2.5 RADAR OBSERVATIONS OF INTENSE OROGRAPHIC PRECIPITATION ASSOCIATED WITH TYPHOON XANGSANE (2000)

Cheng-Ku Yu* and Lin-Wen Cheng

Department of Atmospheric Sciences
Chinese Culture University
Taipei, Taiwan

1. INTRODUCTION

Orographic precipitation can occur in a wide variety of synoptic conditions. However, our understanding on this subject is mainly obtained from the previous studies of the midlatitude wintertime precipitation events developing over the mountainous regions. Two primary factors, the dynamical interaction between the airflow and topography and its associated microphysical processes, have been long recognized to be crucial in determining the intensity and location of precipitation (Smith 1979; Banta et al. 1990; Colle 2004). Particularly, with analyses of detailed Doppler radar measurements collected over mountains from recent field experiments, a number of observational and modeling studies have further explore our knowledge on how the orographically influenced circulations modulate the precipitation associated with midlatitude synoptic disturbances (e.g., Yu and Smull 2000; Neiman et al. 2004; Lin et al. 2005).

In contrast to orographic precipitation associated with midlatitude weather disturbances, which has been largely explored previously, little knowledge on orographic precipitation occurring in typhoon environment has been learned. Fundamentally, the flow regime in typhoon environment would be distinctly different from that associated with midlatitude weather systems such as synoptic fronts and cyclones. Regions in the vicinity of typhoons are usually characterized by abundant moisture and high winds at low levels. This implies a relatively large Froude number that particularly favors orographic lifting and resulting precipitation enhancement. However, the direction and intensity of oncoming flow would change significantly as a typhoon approaches a barrier. The terrain-flow interaction relevant to this aspect, of course, is further complicated by the high variety of precipitation inherently associated with typhoon circulations.

Typhoon circulations interacting with topography are often found to be crucial for contributing to the occurrence of heavy and persistent precipitation over and near mountains (Wu and Kuo 1999; Wu et al. 2002). With the analysis of conventional surface observing data, few past studies have also indicated a significant role of orography in controlling the precipitation patterns and intensities as typhoons passed over a mountain barrier (e.g., Chang et al. 1993). Owing to the lack of adequate observations over the mountainous regions, these previous studies provide only a gross view of such phenomena, and their associated physical processes have not been clearly identified.

In this study, measurements from two ground-based Doppler radars located in northern Taiwan were used to document the detailed aspects of the precipitation distribution and intensity as the typhoon Xangsane (2000) moved northward off the northeastern coast of Taiwan and brought strong low-level northeasterly to north-northeasterly winds impinging on the mountainous northern coast. How these observed spatial and temporal variations of precipitation relate to the topography and upstream airflow was particularly focused in this study. Xangsane is one of the most severe typhoons influencing Taiwan in past years. This event brought extremely heavy rainfall over northern Taiwan, which caused significant property damage and took many people life away (64 death and 25 lost).

2. DATA AND METHODOLOGY

The primary datasets used in this study were provided by the Central Weather Bureau of Taiwan operational S-band Doppler radar (WSR-88D) on Wu-Fen-San (hereafter, WFS) and the Civil Aeronautics Administration (hereafter, CAA) operational C-band Doppler radar located at Chiang Kai-Shek international airport. Locations of these two radars are indicated in Fig. 1. Both radars provide volumetric distributions of reflectivity and radial velocity with a temporal interval of ~6 min (for WFS radar) and ~30 min (for CKS radar) between each volume. Because the WFS radar is situated ~10 km inland from the northern coast, it provides a better data coverage for precipitation occurring over the mountainous regions of northern Taiwan.

* Corresponding author address: Dr. Cheng-Ku Yu,
Dept. of Atmospheric Sciences, Chinese Culture University,
55, Hwa-Kang Road, Yang-Ming-Shan, Taipei 111, Taiwan
E-mail: yuku@faculty.pccu.edu.tw

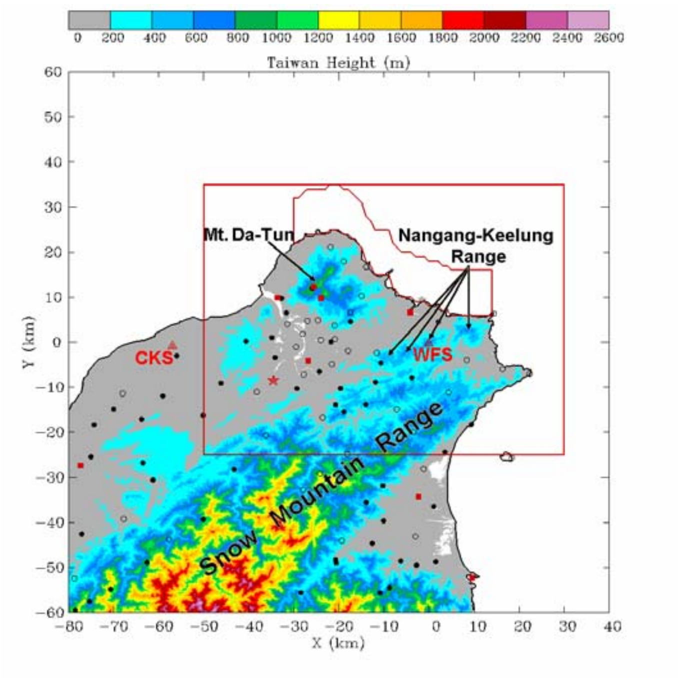

Fig. 1. Topographic features in northern Taiwan. Terrain height (m MSL) is indicated by shading (key at top). Locations of the Doppler radar site at Wu-Fen-San (WFS) and Chiang Kai-Shek (CKS) international airport are denoted by the triangle. Locations of surface observing stations, automatic meteorological observing stations, automatic rain gauge, and sounding station are denoted by squares, hollow circles, solid circles, and asterisk, respectively. The red contour denotes the region for calculating the mean dual-Doppler synthesized winds upstream of Taiwan island. The red box indicates the main domain of this study.

In this study, the dual-Doppler synthesis of the WFS and CKS radars was also applied to retrieve the kinematic information off the northern coast of Taiwan, upstream of the barriers. Other data sources used in this study, including routine surface and sounding observations, are indicated in Fig. 1.

3. CASE OVERVIEW

Typhoon Xangsane (2000) initially moved westward after its formation over the tropical western Pacific Ocean on 26 October 2000. It headed north immediately west of Philippine on 30 October 2000 (Fig. 2) and kept its northward journey over Bashi Channel in the next two days. Xangsane did not make landfall on the landmass of Taiwan but passed nearshore along the eastern coast of Taiwan during 31 October to 1 November 2000.

During the passage of Xangsane, heavy rain was observed and appeared to be persistent over the northern Taiwan. Figure 3 shows the 0329 UTC 1 November PPI display of radar reflectivity and radial velocity at 1.4^{o} elevation from the WFS radar. During this time, Xangsane's center with near-zero reflectivities was located ~60 km offshore east of northern Taiwan and primary precipitation associated with the typhoon circulation was confined to regions north and west of the typhoon center (Fig. 3a). The outer typhoon precipitation bands typically moved onshore and made landfall on the

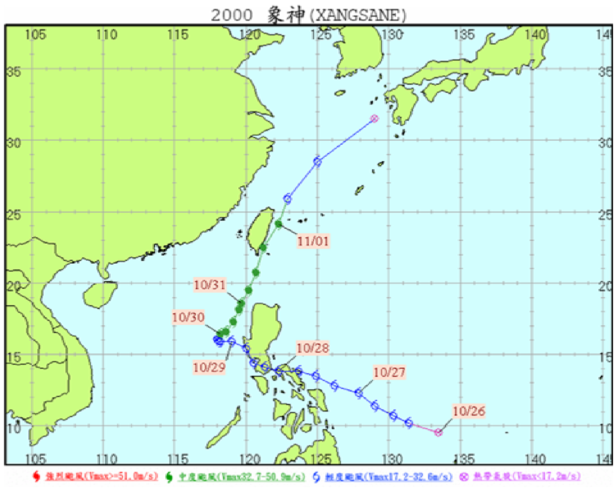

Fig. 2. Track of typhoon Xangsane (2000). Typhoon center is indicated at every 6-h.

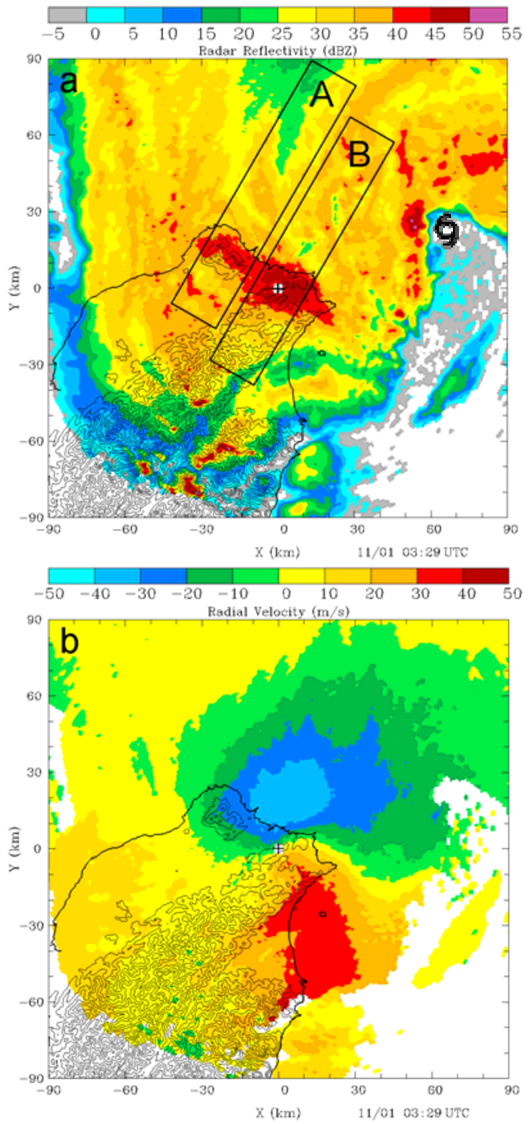

Fig. 3. Low-level PPI scan (1.4^{o} elevation) from the WFS radar (location marked by +) at 0329 UTC 1 November 2000. (a) radar reflectivity (dBZ). (b) radial velocity (m s^{-1}). Terrain height is indicated by contours with a 300-m interval. Two inset elongated boxes encompassing the DT and SMR indicate the area for calculating a mean radar reflectivity along the box shown in Fig. 4.

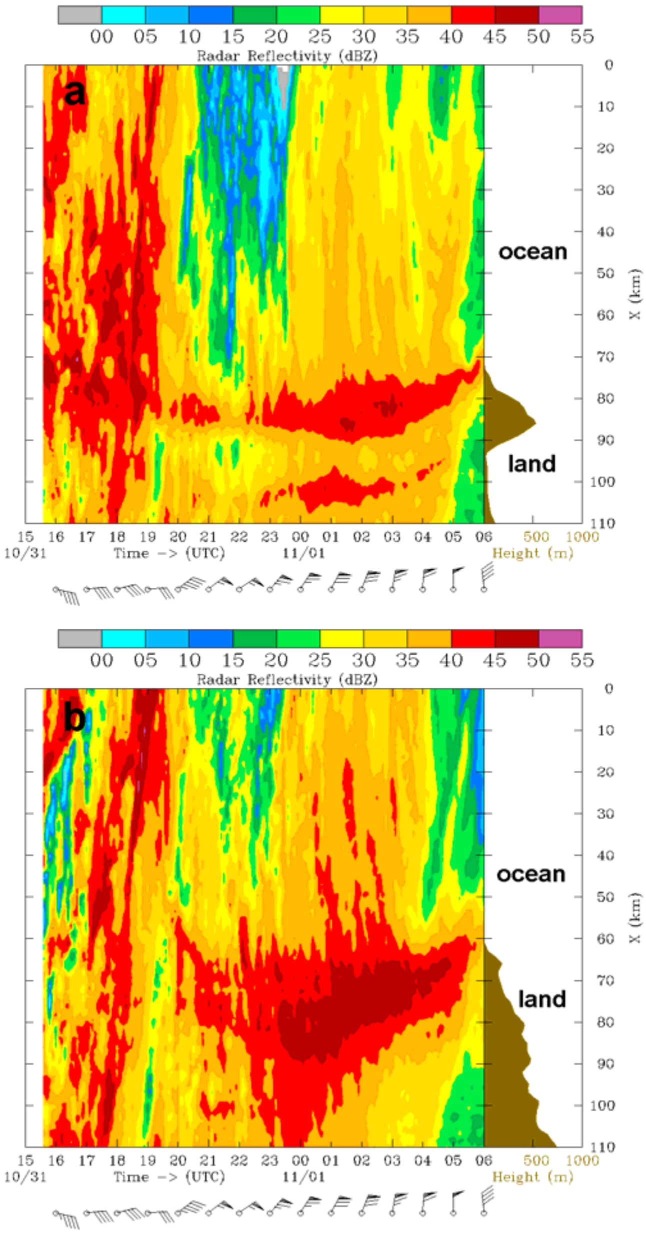

Fig. 4. Temporal variation of precipitation in the vicinity of northern Taiwan during 1500 UTC 31 October to 0600 UTC 1 November 2000. The low-level PPI scan (1.4° elevation) of radar reflectivity from the WFS radar within the elongated boxes (shown in Fig. 3) was averaged in a direction normal to the orientation of the box and plotted as a function of time and along-box distance. Results for box A and B are shown in (a) and (b), respectively. On the right panel of each figure, corresponding mean terrain height along the box. Low-level mean dual-Doppler synthesized winds (averaged below 2 km over the upstream area indicated in Fig. 1) are also indicated (full wind barbs correspond to 5 m s^{-1}; half barbs to 2.5 m s^{-1}).

northern coast of Taiwan. Northerly winds associated with typhoon circulations characterized by intense approaching radial velocities (greater than 30 m s^{-1}) prevailed immediately upstream of Taiwan landmass (Fig. 3b). Typhoon eyewall with maximum reflectivities reaching above 40-45 dBZ were also evident in offshore regions surrounding the typhoon center.

The strongest precipitation were, however, observed immediately inland along the northern coast of Taiwan, namely adjacent to and over the windward slopes of Mt. Da-Tun (hereafter, DT) and the northmost portion of Snow Mountain Range (hereafter, SMR). This mountainous precipitation appeared to be quasi-stationary, distinct from the fast-moving characteristics of typhoon rainbands. This aspect can be best illustrated by a sequence of low-level radar reflectivities averaged within the elongated boxes (locations in Fig. 3a) encompassing the two mountain barriers and approximately parallel to the oncoming north-northeasterly flow, as shown in Fig. 4. Before 2000 UTC 31 October, the northern Taiwan was mainly influenced by the passage of outer typhoon rainbands with heavy precipitation extending from inland to regions well offshore. No obvious evidence of orographically enhanced precipitation was observed during this early period. However, with the approach of Xangsane the low-level oncoming winds in northern Taiwan became northeasterly after 2000 UTC. Coastal precipitation was significantly enhanced and the heaviest precipitation tended to stay over the windward slopes of mountains. The orographic precipitation started to weaken in association with the decrease in the oncoming northerly flow after 0300 UTC as Xangsane moved farther away from the northern coast of Taiwan. Persistent and intense precipitation over the two mountain barriers caused a significant amount of accumulated rainfall greater than 400 mm over a 10-h period from 2000 UTC 31 October to 0600 UTC 1 November (not shown).

4. CHARACTERISTICS OF HORIZONTAL PRECIPITATION DISTRIBUTION

As described in section 3, the occurrence of significant orographic precipitation was confined to between 2000 UTC 31 October and 0600 UTC 1 November, and hence, analyses of radar observations will be focused only on this 10-h interval. Figure 5a shows the horizontal distribution of accumulated reflectivity from the WFS radar during this period. Distinct precipitation patterns were observed in the vicinity of the two primary mountain barriers. Two precipitation maxima (~4000 dBZ) were observed over the windward slopes of DT but with a sharp decrease in precipitation near mountain peaks and on the lee, leading to a local precipitation minimum located at low foothills southwest of the barrier. Another precipitation maximum with magnitudes (> 4300 dBZ) greater than those seen over DT was found over the first, northern hill of SMR called Nangang-Keelung Range (hereafter, NKR). Note that, in contrast to the precipitation distribution over DT, maximum precipitation with the contour of 4300 dBZ spillover into the lee of NKR was evident. Gradually reduced precipitation was however observed over farther inland, higher mountains.

Figure 5b shows the frequency distribution of strong reflectivity greater than 40 dBZ during the 10-h period.

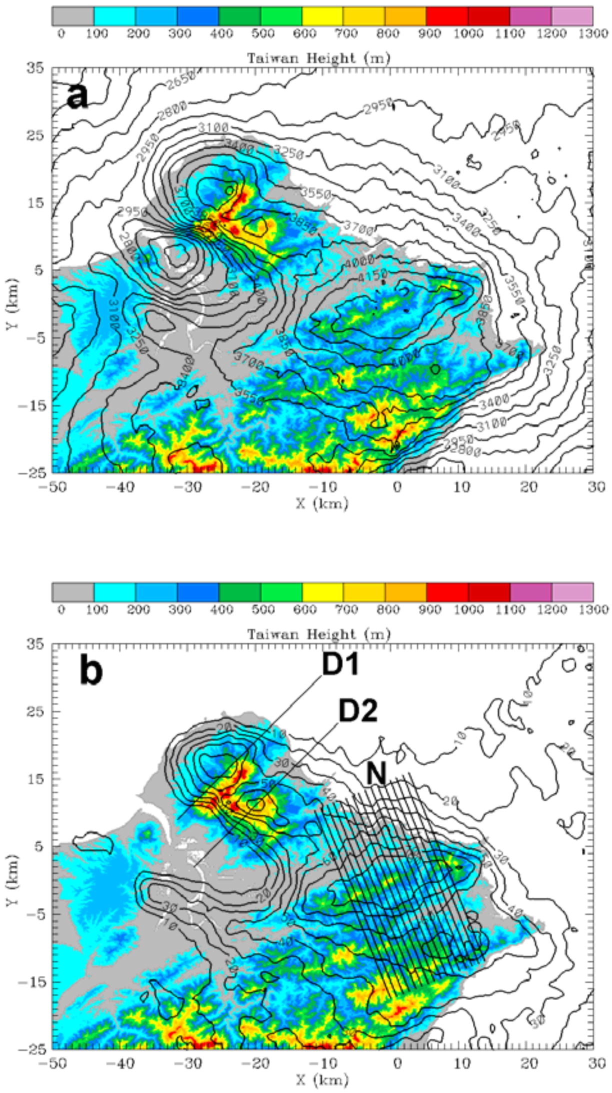

Fig. 5. (a) Horizontal pattern of cumulative reflectivity (contours with 150-dBZ interval) derived from the low-level PPI scan (1.4^{o} elevation) of the WFS radar during the 10-h period from 2000 UTC 31 October to 0600 UTC 1 November 2000. Terrain height (m MSL) is indicated by color shading. (b) As in (a) except showing the frequency distribution of heavy precipitation (>40 dBZ) with contour interval of 10%. Line segment D1, D2 and N mark location of vertical cross sections shown in Figs. 7-9.

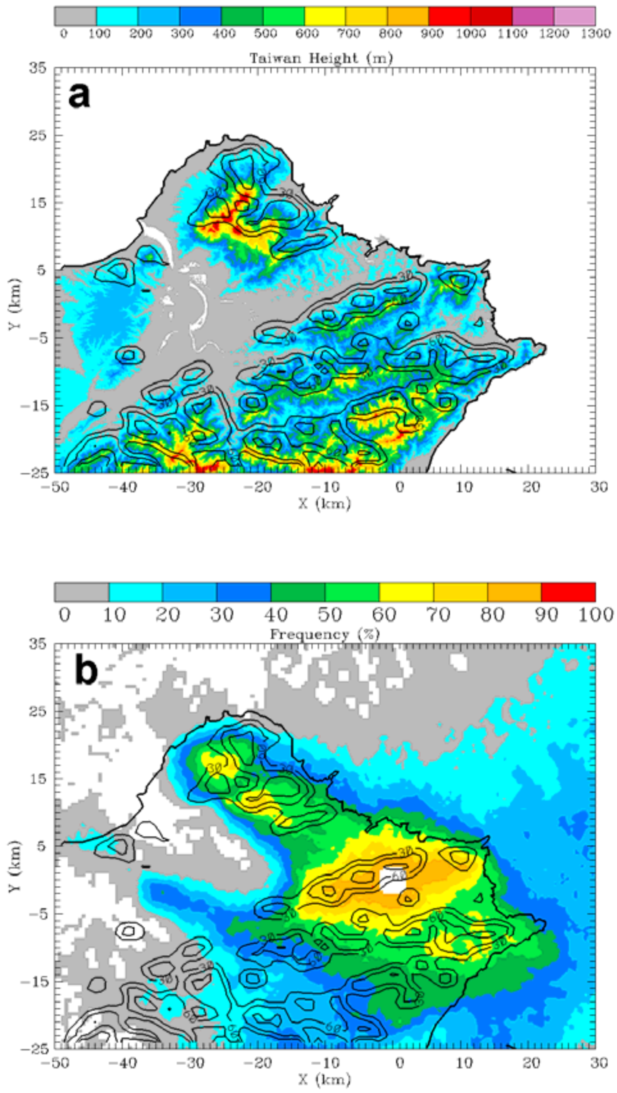

Fig. 6. (a) Frequency distribution of topographically forced vertical motions (>1 m s^{-1}) during the 10-h period from 2000 UTC 31 October to 0600 UTC 1 November 2000, with contour interval of 30%. Color shading indicates terrain height (m MSL). (b) As in (a) except that color shading indicates the frequency distribution of heavy precipitation (>40 dBZ) (shading key at top).

The frequency distributions are highly similar to the pattern of accumulated reflectivity shown in Fig. 5a. Two localized maxima with frequency of 60-70% were found over DT. Largest frequency of heavy precipitation was located over NKR and can reach above 80%, suggesting precipitation over this mountain range to be more intense and stably persistent. As will be described later, a relatively large frequency found over this narrow barrier is consistent with the quasi-stationary characteristics of heavy precipitation and the influences by the landfalling typhoon rainbands.

An interesting but uncertain issue regards whether the distributions of orographically enhanced precipitation as shown in Fig. 5 have some physical connections to the topographically forced vertical motions. Considering the horizontal winds flowing over a mountain, the topographically forced vertical velocity is proportional to the steepness of mountain slope along the wind direction of oncoming flow and can be approximated by the expression:

$$W_{terrain}(x,y,t) = u(h,t)\frac{\partial h(x,y)}{\partial x} + v(h,t)\frac{\partial h(x,y)}{\partial y} \qquad (1)$$

where h is the terrain height, and u and v represent the east-west and south-north flow components of upstream oncoming winds, respectively. Equation (1) has been used in many previous studies to evaluate the relative importance of orographic lifting and other convective forcings associated with synoptic and/or mesoscale systems (e.g., Lin et al. 2001; Neiman et al. 2002; Wu et al. 2002; Georgis et al. 2003). In order to obtain more representative magnitudes for $W_{terrain}$ at different slope heights and time, u and v in (1) are not a constant value but a function of the terrain height h and time. In our calculations, u and v values at different time periods are obtained from dual-Doppler synthesis winds averaged within an upstream area (indicated in Fig. 1).

Figure 6 shows the frequency distribution of $W_{terrain}$ greater than 1 m s^{-1}. In consistence with prevailing north-northeasterlies, regions of large frequency values were generally found over the northern slopes of mountains (Fig. 6a). The narrow zone of the most enhanced precipitation over NKR generally coincided very well with the maximum frequency of vertical motions (Fig. 6b) except for the leeside precipitation. There was less evidence of significant precipitation enhancement associated with the cores of maximum frequency of vertical motions over farther inland (i.e., more southern) slopes and ranges of SMR. In addition, regions of two precipitation maxima over DT did not coincide with the largest frequency of vertical motions, but they still tend to be located near and immediately downstream of these local maxima of frequency.

5. RELATION OF PRECIPITATION TO TOPOGRAPHY AND UPSTREAM CONDITIONS

A sequence of radar observations during the period of interest indicated that the intensity and location of enhanced precipitation over DT and NKR did evolve considerably with the changes in upstream oncoming flow associated with typhoon circulations. Some vertical cross sections across the major regions of orographic precipitation are presented herein to illustrate these important aspects. For the three-dimensional and wider barrier (~8 km in slope width) of DT, two vertical sections (D1 and D2 indicated in Fig. 5b) are selected to pass through the cores of heaviest precipitation and to be oriented approximately parallel to the oncoming flow. For the approximately two-dimensional and narrower barrier (only ~4 km in slope width) of NKR, several vertical sections (N indicated in Fig. 5b) running through the region of heaviest precipitation and normal to the barrier are selected. A representative vertical cross section is then obtained by averaging these different, respective vertical sections. Note that, given a roughly two-dimensional precipitation pattern over NKR (cf. Fig. 5), precipitation structures seen from individual vertical sections are highly similar to those of the calculated mean vertical section. Radar reflectivities along each of selected sections (i.e., D1, D2, and N) observed from different time periods are also averaged within an interval (5 m s^{-1} used herein) of oncoming wind component parallel to the section ranging from 0 m s^{-1} to 35 m s^{-1}. These results from the vertical section D1, D2, and N are shown in Figs. 7-9, respectively.

Over DT, when the oncoming flow increased, the location of low-level precipitation maximum tended to shift obviously toward the mountain crest from regions slightly upstream of the mountain or over lower mountain slopes, and the low-level strongest reflectivities also increased from 42-43 dBZ at relatively weak oncoming flow regime to 45-46 dBZ at stronger oncoming flow regime (Figs. 7 and 8). Vertical extent of heavy precipitation (>40 dBZ) was generally confined to the lowest 2.5 km (MSL) but it became slightly deeper (with the 40 dBZ contour reaching above 2 km) at stronger oncoming flow regime (>25 m s^{-1}). In contrast to the precipitation features observed over DT, the region of low-level precipitation maximum over NKR was not observed over the windward slope and instead, it tended to be located near the mountain crest, with a trend to move slightly toward the lee as oncoming flow increased (Fig. 9). Note that the degree of this downstream shift of low-level heavy precipitation (≤~5 km) was relatively limited, compared to a larger downstream shift (≥~10 km) observed over DT (cf. Figs. 7 and 8). This aspect can be more clearly seen if the lowest-level reflectivity along the selected vertical cross sections is plotted as a function of oncoming flow component, as shown in Fig. 10.

Similar to DT, there was some evidence of precipitation enhancement when oncoming flow intensified and the most enhanced precipitation was also confined to the lowest level (Fig. 9). Consistent with analyses presented in Fig. 5a showing larger accumulated reflectivity values over NKR than over DT, the low-level precipitation with maximum generally greater than 45 dBZ was found. However, the vertical extent of heavy precipitation was obviously higher than that observed over DT. The 40 dBZ contour extending from the ground to a height of at least 4 km was observed, except for the vertical cross section shown in Fig. 9a where its corresponding cross-barrier flow components were pretty small (<5 m s^{-1}).

It is noteworthy that, as shown in Fig. 3a, the larger-scale area of considerable precipitation associated with Xangsane were present. The precipitation bands embedded within the typhoon circulations, as they made landfall, would interact with topography to further modify precipitation developing over mountains. This kind of interaction appears to be more pronounced over NKR because the majority of the offshore intense typhoon rainbands approached and encountered this barrier (Fig. 4b). Analyses (not shown) indicate that, with the landfall of these typhoon rainbands, the pre-existing precipitation over NKR was further intensified and its vertical extent also became much deeper. In addition to the contrasting mountain geometry between the DT and NKR, the influences of landfalling typhoon rainbands are believed to contribute partly to the observed differences in precipitation characteristics over these two barriers.

6. CONCLUSIONS

The detailed aspects of precipitation distribution and

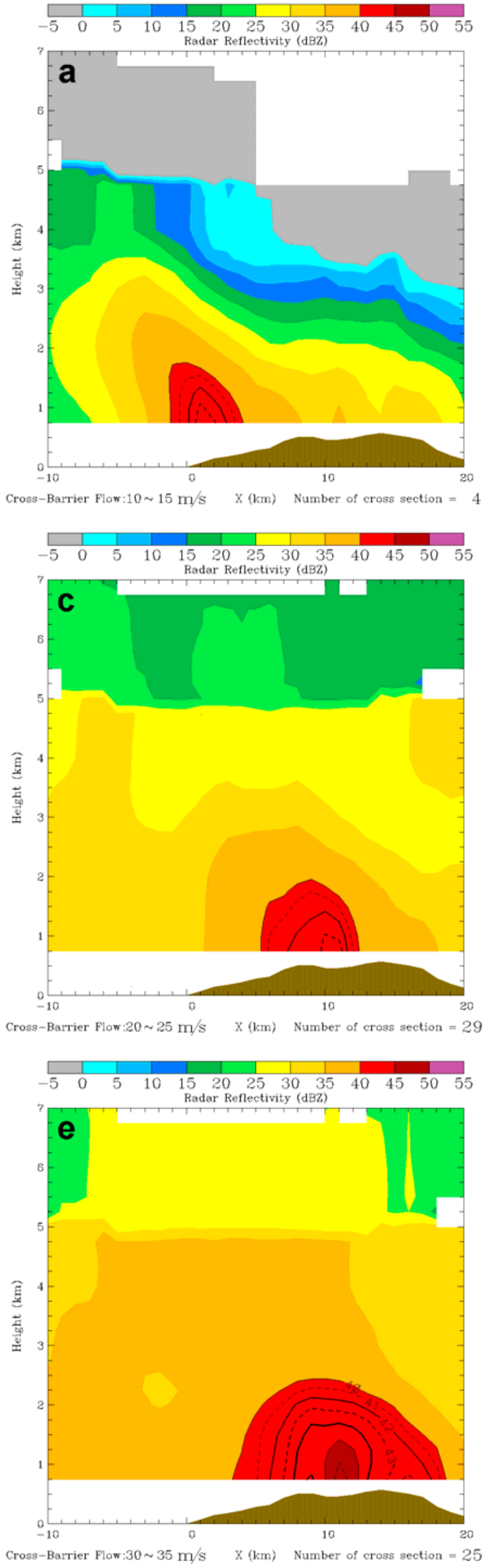

Fig. 7. Mean vertical patterns of reflectivity (dBZ, color shading) along D1 in Fig. 5b, obtained from different intervals of low-level oncoming wind component along the section. (a) to (e) corresponding to the oncoming flow at 10-15, 15-20, 20-25, 25-30, and 30-35 m s^{-1}, respectively. Regions having reflectivity higher than 40 dBZ are also contoured at an interval of 1 dBZ. Shading in lower portion of each panel indicates topography along the section.

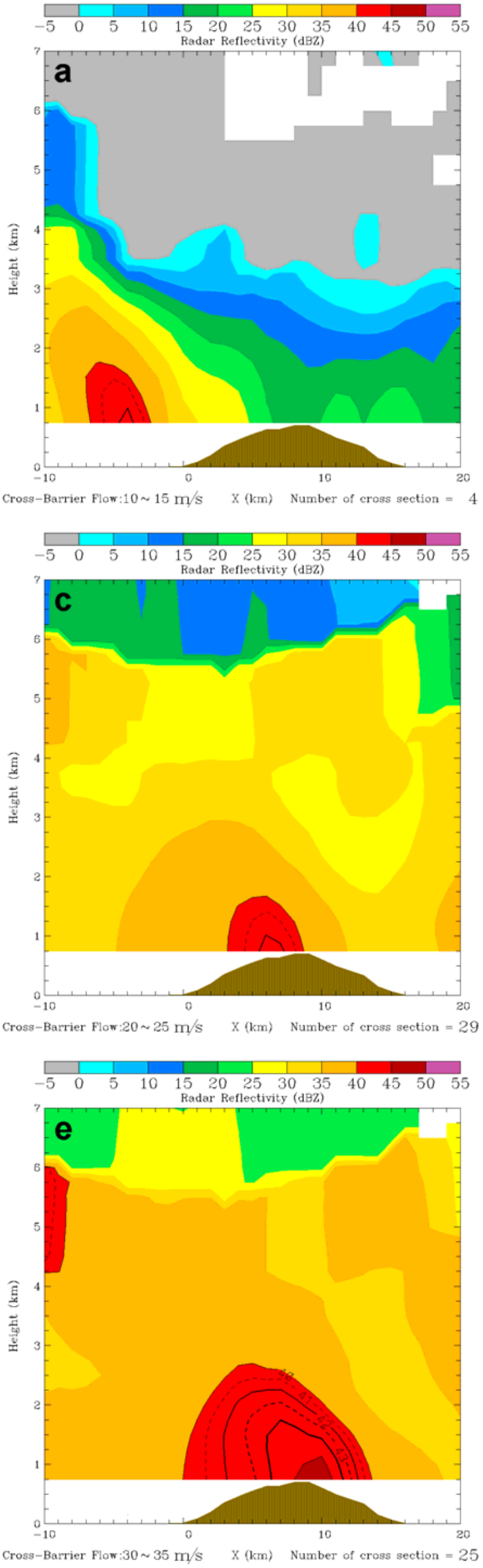

Fig. 8. As in Fig. 7 except along D2 in Fig. 5b.

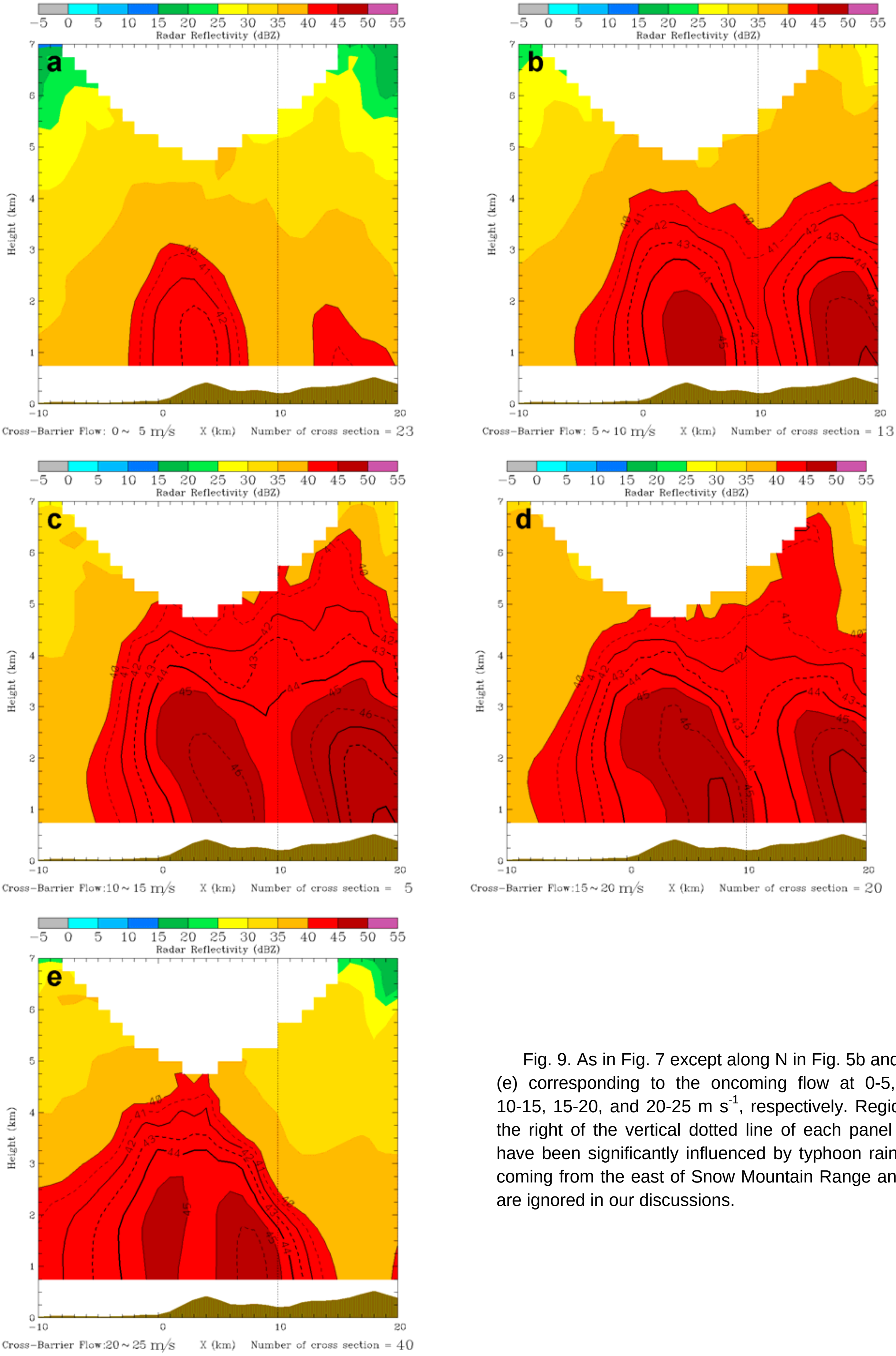

Fig. 9. As in Fig. 7 except along N in Fig. 5b and (a) to (e) corresponding to the oncoming flow at 0-5, 5-10, 10-15, 15-20, and 20-25 m s^{-1}, respectively. Regions on the right of the vertical dotted line of each panel would have been significantly influenced by typhoon rainbands coming from the east of Snow Mountain Range and thus are ignored in our discussions.

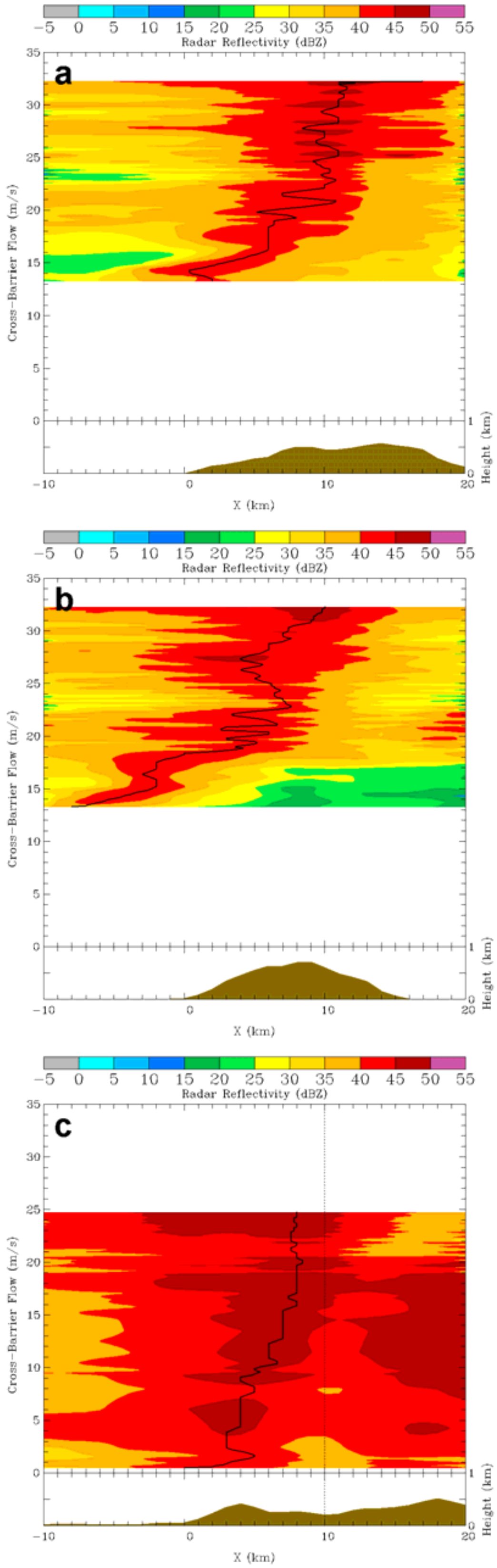

Fig. 10. (a) to (c) display the lowest-level (750 m MSL) reflectivity (dBZ, color shading) of the WFS radar along D1, D2, and N in Fig. 5b, respectively, as a function of oncoming flow component. Thick heavy contour in each panel denotes location of strongest radar reflectivity found at a given oncoming flow component. Shading in lower portion of each panel indicates topography along the section.

intensity over the mountainous regions in northern Taiwan as the typhoon Xangsane (2000) moved northward off the northeastern coast of Taiwan and brought strong low-level northeasterly to north-northeasterly winds impinging on the mountainous northern coast have been documented using measurements from two ground-based Doppler radars located in northern Taiwan. In northern Taiwan, there are two primary mountain barriers; one is the DT, a complicated three-dimensional mountain barrier with peak mountain heights of ~1000 m and a slope width of ~8 km, and the other, the northern portion of Snow Mountain Range with relatively lower and narrower two-dimensional hills oriented roughly southwest-northeast, adjacent to the southeast of the DT. Analyses of accumulated radar reflectivity revealed two precipitation maxima located over the windward slopes of DT but with a sharp decrease in precipitation near mountain peaks and on the lee, leading to a local precipitation minimum located at low foothills southwest of the barrier. Another precipitation maximum with even larger accumulated reflectivity values was found near the first, northern hill (i.e., NKR, with a slope width of only ~4 km) of SMR. Particularly, the zone of the heaviest precipitation spillover into the lee of this narrow barrier was also evident.

Analyses of vertical cross sections passing through the major precipitation regions suggest the importance of oncoming winds on influencing the precipitation location relative to topography and its associated intensity. It is also clear that the behavior of orographically enhanced precipitation over these two distinct barriers (DT and NKR) in terms of its location, intensity, and vertical structure is inherently different. These aspects mainly include a deeper (shallow) vertical extent of heavy precipitation, a stronger (weaker) intensity of low-level precipitation, and a shorter (longer) distance of the downstream shift with respect to different magnitudes of oncoming winds over the NKR (DT). Observations suggest that the contrasting mountain geometry of the DT and NKR and the different degree of influences of typhoon rainbands are two primary factors contributing to the observed differences in precipitation characteristics over these two barriers.

Acknowledgments. This research has been supported by the National Science Council of the Republic of China under Grant NSC 95-2111-M-034-001.

REFERENCES

Banta, R. M., and Coauthors, 1990: *Atmospheric Processes over Complex Terrain. Meteor. Monogr.*, No. 45, Amer. Meteor. Soc., 323 pp.

Chang, C.P., T. C. Yeh, and J. M. Chen, 1993：Effects of terrain on the surface structure of typhoons over Taiwan. *Mon. Wea. Rev.*, **121**, 734-752.

Colle, B. A. , 2004：Sensitivity of orographic precipitation to changing ambient conditions and terrain geometries：An idealized modeling perspective. *J. Atmos. Sci.* , **61**, 588-606.

Georgis, J.-F., F. Roux, M. Chong, and S. Pradier, 2003: Triple-Doppler radar analysis of the heavy rain event observed in the Lago Maggiore region during MAP IOP 2b. *Quart. J. Roy. Meteor. Soc*., **129**, 495-522.

Lin, Y.-L., S. Chiao, T.-A. Wang, M. L. Kaplan, and R. P. Weglarz, 2001: Some common ingredients for heavy orographic rainfall. *Wea. Forecasting.,* **16**, 633–660.

Lin, Y.- L., H. D. Reeves, S.- Y. Chen, and S. Chiao, 2005: Formation mechanisms for convection over the Ligurian Sea during MAP IOP-8. *Mon. Wea. Rev.*, **133**, 2227-2245.

Neiman, P. J., F. M. Ralph, A. B. White, D. E. Kingsmill, and P. O. G. Persson, 2002: The statistical relationship between upslope flow and rainfall in California’s coastal mountains: Observations during CALJET. *Mon. Wea. Rev*., **130**, 1468-1492.

Neiman, P. J., P. O. G. Persson, F. M. Ralph, D. P. Jorgensen, A. B. White, and D. E. Kingsmill, 2004: Modification of fronts and precipitation by coastal blocking during an intense landfalling winter storm in southern California: Observations during CALJET. *Mon. Wea. Rev*., **132**, 242-273.

Smith, R. B., 1979: The influence of mountains on the atmosphere. *Advances in Geophysics*, **21**, Academic Press, 87-230.

Wu, C.- C., and Y.- H. Kuo, 1999: Typhoons affecting Taiwan: Current understanding and future challenges. *Bull. Amer. Meteor. Soc.*, **80**, 67-80.

Wu, C.- C., T.- H. Yen, Y.- H. Kuo, and W. Wang., 2002: Rainfall simulation associated with typhoon Herb (1996) near Taiwan. Part I: The topographic effect. *Wea. Forecasting*, **17**, 1001–1015.

Yu, C.- K., and B. F. Smull, 2000: Airborne Doppler observations of a landfalling cold front upstream of steep coastal orography. *Mon. Wea. Rev*., **128**, 1577-1603.